



PAPER

Enhanced two-photon emission from a dressed biexciton

Carlos Sánchez Muñoz¹, Fabrice P Laussy^{1,2}, Carlos Tejedor¹ and Elena del Valle¹¹ Departamento de Física Teórica de la Materia Condensada and Condensed Matter Physics Center (IFIMAC), Universidad Autónoma de Madrid, 28049, Spain² Russian Quantum Center, Novaya 100, 143025 Skolkovo, Moscow Region, RussiaE-mail: elena.delvalle.reboul@gmail.com**Keywords:** biexciton, two-photon emitters, entangled photons, resonance fluorescence, radiative cascade, quantum dot, microcavitySupplementary material for this article is available [online](#)

RECEIVED

30 June 2015

REVISED

11 November 2015

ACCEPTED FOR PUBLICATION

17 November 2015

PUBLISHED

15 December 2015

Content from this work
may be used under the
terms of the [Creative
Commons Attribution 3.0
licence](#).

Any further distribution of
this work must maintain
attribution to the
author(s) and the title of
the work, journal citation
and DOI.



Abstract

Radiative two-photon cascades from biexcitons in semiconductor quantum dots under resonant two-photon excitation are promising candidates for the generation of photon pairs. In this work, we propose a scheme to obtain two-photon emission that allows us to operate under very intense driving fields. This approach relies on the Purcell enhancement of two-photon virtual transitions between states of the biexciton dressed by the laser. The richness provided by the biexcitonic level structure allows to reach a variety of regimes, from antibunched and bunched photon pairs with polarization orthogonal to the driving field, to polarization entangled two-photon emission. This provides evidence that the general paradigm of two-photon emission from a ladder of dressed states can find interesting, particular implementations in a variety of systems.

1. Introduction

The generation of non-classical states of light is a major goal in the implementation of photonic quantum technologies [1, 2]. A case of particular interest is the generation of photon pairs, since they present a wide range of applications in quantum information and quantum communications [3]. Photon pairs are an important resource with which to generate heralded single photons [4] and are also used in quantum key distribution [5, 6], quantum teleportation [7, 8] or to implement entanglement swapping and quantum repeaters [9–11]. Numerous other examples, like quantum lithography [12], the absorption rate increase from organic molecules in two-photon microscopy [13, 14], quantum walks of correlated photons [15] or the quantum computation of molecular properties [16], illustrate the rich variety of applications that these non-classical states of light can find.

Despite having such an impressive number of applications, the number of ways in which these states can be generated is limited: most sources of photon pairs employed to date are based on parametric down-conversion [3, 7, 16–18]. This mechanism can be implemented in several platforms, and thankfully for prospective technologies, semiconductors have demonstrated excellent performances [19–21]. These sources suffer however from the major drawback that the number of photon pairs generated in each process shows Poissonian statistics, with a non-zero probability of having zero pairs or more than one pair [22]. Promising candidates to overcome this difficulty are quantum emitters that naturally emit entangled photon pairs in a radiative cascade [23]. In the semiconductor case, the biexciton $|B\rangle$ in a quantum dot offers such an implementation, and emission of entangled photon pairs from the biexcitonic cascade has been demonstrated in recent years [24–28]. As an alternative to off-resonant excitation, it is possible to initialize the biexcitonic state by coherent two-photon excitation (TPE) [28–32], which increases the coherence and indistinguishability of the emitted photons as compared to non-resonant pumping. The generation efficiency and the indistinguishability of the photons can also be improved by bringing a cavity in resonance with the biexcitonic transition [27] to enhance the emission thanks to the Purcell effect [33]. A particularly interesting possibility is to place the cavity in resonance with half the energy of the biexciton to enhance the rate of spontaneous two-photon emission, such that two photons are emitted simultaneously into the cavity mode [34–36]. The joint implementation of

coherent excitation and Purcell enhancement via cavity modes has already been discussed in the literature and shown to be promising [28, 35].

Under coherent excitation, the intensity of the pumping sets a limit to the repetition rate of two-photon generation, since strong driving fields dress the excitons and spoil the biexcitonic structure [37, 38]. On the other hand, a recent proposal [39] took advantage of such a dressing and demonstrated that a continuous source of N -photon states—with photon pairs as the simplest realization—can be achieved in precisely this regime of strong admixing of the exciting laser with the emitter. This relies on a family of virtual two-photon transitions, so-called *leapfrog* processes [40], in the strong driving of resonance fluorescence. Since virtual two-photon states are emitted away from the fluorescence peaks, they have a very small probability of occurring on their own. These elusive photons are however precious [41] since they feature giant quantum correlations and violate classical inequalities [42]. Despite their scarcity, their existence has recently been demonstrated experimentally by measurements of frequency-resolved photon correlations [43]. It is therefore timely to capitalize on these photons by devising bright, continuous sources of photon pairs by harvesting them with a cavity mode, with a Purcell-effect applied similarly to previous enhancements of quantum correlations [44, 45] from real photons emitted at the sidebands [46–48].

In this work, we bring together the three main ideas exposed above: (i) TPE from the biexciton, (ii) cavity Purcell enhancement of virtual processes and (iii) multiphoton emission from a dressed system. This realizes a versatile two-photon source operating in the continuous regime with a high repetition rate. In comparison with the case of a single dressed two-level system, the biexciton introduces an extra degree of freedom, the polarization, which provides a richer set of physical regimes. In particular, we demonstrate the emission of degenerate photon pairs with polarization orthogonal to the laser—therefore suppressing the laser background and undesired excitation of the cavity—and different two-photon counting statistics, as well as emission of polarization-entangled photons. All these different regimes can be accessed optically with the same sample just by changing the intensity and polarization of the excitation. This unprecedented versatility will push forward the generation and use of photon pairs in the laboratory. Even more importantly, it provides evidence that the fundamental concepts are susceptible to application in different platforms, such as superconducting circuits [49], and that new regimes of non-classical light emission are within reach with variations of the design.

Our analysis starts with a general introduction of the model in section 2, and follows with a detailed description of the features of the dressed biexciton alone in terms of its single and two-photon spectrum of emission, in sections 3 and 4 respectively. In section 5, we present the complete picture with the inclusion of a cavity that probes and enhances the single and two-photon transitions from the dressed system. In section 6, we show how this system can efficiently generate polarization and frequency (or time) entangled photon pairs. Finally, in section 7, we present our conclusions.

2. Model and dressed state picture

The system under consideration is a semiconductor quantum dot with a biexcitonic structure, as depicted in figure 1(a). It can host two excitons, or electron–hole pairs, with third component of the total angular momentum equal to $+1$ or -1 , usually labelled as ‘spin states’. Symmetric and antisymmetric combinations of these states couple to one of the two orthogonal linearly polarized light modes (‘vertical’ and ‘horizontal’). The biexciton state corresponds to the occupation of both spin states in the dot. The Hamiltonian of this system is given by

$$H_X = \omega_X (\sigma_\uparrow^\dagger \sigma_\uparrow + \sigma_\downarrow^\dagger \sigma_\downarrow) - \chi (\sigma_\uparrow^\dagger \sigma_\uparrow \sigma_\downarrow^\dagger \sigma_\downarrow), \quad (1)$$

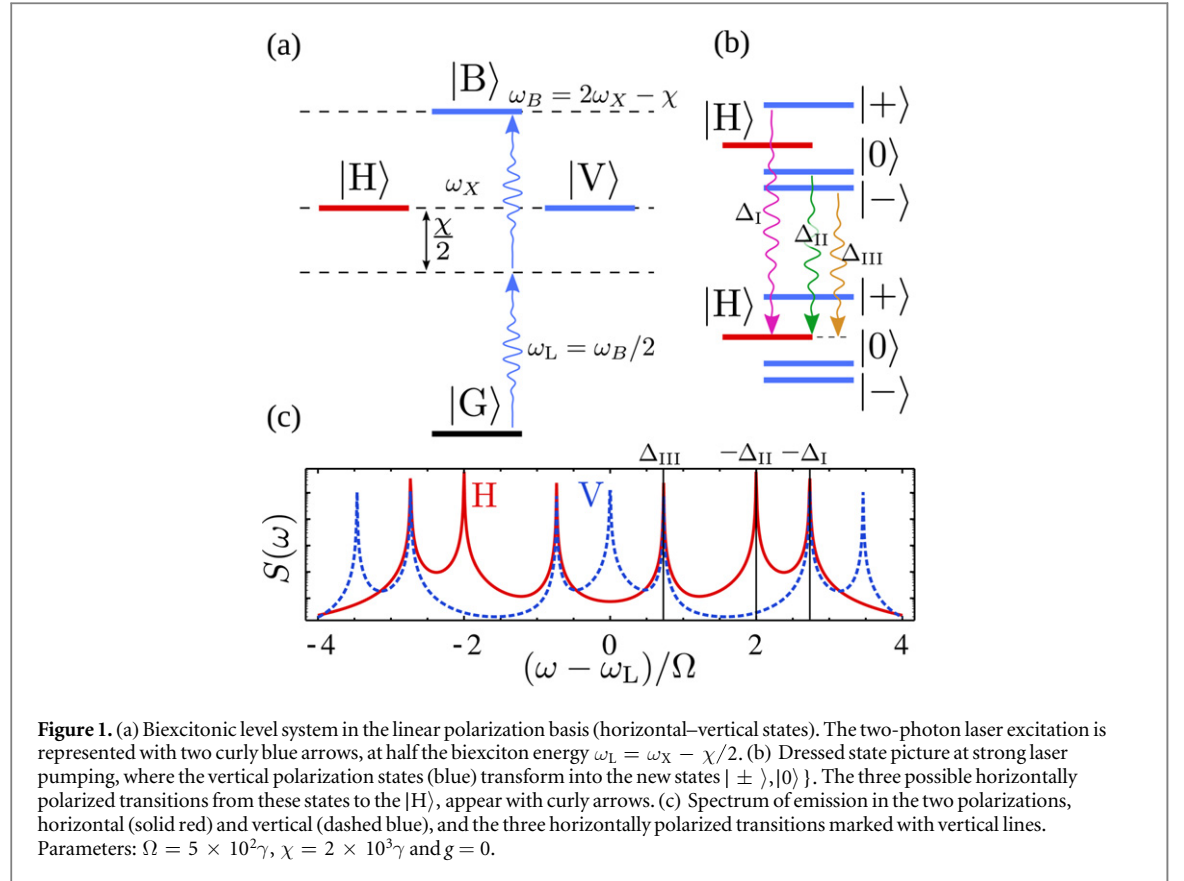
where $\{\sigma_\uparrow, \sigma_\downarrow\}$ are the annihilation operators of the excitons with spin $\{\uparrow, \downarrow\}$, ω_X is the excitonic energy (we consider degenerate excitons) and χ is the biexcitonic binding energy. The biexciton frequency is, therefore, $\omega_B = 2\omega_X - \chi$. Note that we have set $\hbar = 1$ hereafter for simplicity. In order to separate the four-level system into two different polarization cascades we change to the linear polarization basis:

$$|H\rangle = \frac{1}{\sqrt{2}}(|\uparrow\uparrow\rangle + |\downarrow\downarrow\rangle), \quad |V\rangle = \frac{1}{\sqrt{2}}(|\uparrow\uparrow\rangle - |\downarrow\downarrow\rangle) \quad (2)$$

with the annihilation operators

$$\sigma_H = \frac{1}{\sqrt{2}}(\sigma_\uparrow + \sigma_\downarrow), \quad \sigma_V = \frac{1}{\sqrt{2}}(\sigma_\uparrow - \sigma_\downarrow). \quad (3)$$

These operators describe transitions from the biexciton to an excitonic state or from an exciton to the ground state by emission of photons with the corresponding horizontal or vertical polarization (red and blue colors in figure 1). We will neglect the small fine structure splitting in frequency that is usually found between the



two different excitonic states, since it has no impact in our scheme and only complicates the algebra. It can be trivially added if needed.

We implement a continuous resonant excitation of this level structure that affects only one of the polarizations (chosen to be the vertical one without loss of generalization). This is accounted for by a coherent driving term in the Hamiltonian:

$$H_\Omega = \Omega (\sigma_V^\dagger e^{-i\omega_L t} + \sigma_V e^{i\omega_L t}) \quad (4)$$

where the intensity of the laser is proportional to $|\Omega|^2$. In order to drive the biexciton state directly, the laser frequency is set at the two-photon resonance, $\omega_L = \omega_B/2$. This results in a two-photon excitation (TPE) to the biexciton level [28–32]. On the other hand, we gather and enhance the emission in the perpendicular polarization (horizontal) through the coupling to a cavity mode with the same linear polarization. This way, we completely separate in polarization the excitation and emission channels and do not need to worry about the elastically scattered light from the laser. The coupling to the cavity mode is given by the Hamiltonian term:

$$H_C = \omega_C a^\dagger a + g (a^\dagger \sigma_H + a \sigma_H^\dagger). \quad (5)$$

We write the total Hamiltonian in the rotating frame of the exciting laser:

$$\begin{aligned} H &= H_X + H_\Omega + H_C \\ &= \Delta_X (\sigma_H^\dagger \sigma_H + \sigma_V^\dagger \sigma_V) - \chi \sigma_H^\dagger \sigma_H \sigma_V^\dagger \sigma_V + \Omega (\sigma_V^\dagger + \sigma_V) \\ &\quad + \Delta_C a^\dagger a + g (a^\dagger \sigma_H + a \sigma_H^\dagger) \end{aligned} \quad (6)$$

where $\Delta_X = \omega_X - \omega_L$ and $\Delta_C = \omega_C - \omega_L$. The dynamics of the whole system is described by a density matrix which follows the master equation:

$$\dot{\rho} = -i[H, \rho] + \frac{\kappa}{2} \mathcal{L}_a \rho + \frac{\gamma}{2} \sum_{X=H,V} [\mathcal{L}_{|X\rangle\langle B|} + \mathcal{L}_{|G\rangle\langle X|}] \rho \quad (7)$$

where we use the definition of the Lindblad term:

$$\mathcal{L}_O \rho = 2O\rho O^\dagger - O^\dagger O \rho - \rho O^\dagger O, \quad (8)$$

and the excitonic and cavity lifetimes are given by γ and κ respectively. We study the steady state of the system defined by $\dot{\rho} = 0$.

Under TPE ($\Delta_X = \chi/2$), the energy of the photons from the laser matches half the biexciton energy, cf figure 1(a). To understand the spectral features of the system before coupling it to the cavity ($g = 0$), we derive a dressed state picture for the biexciton [37]. The starting point is the set of bare states with n excitations, $\{|G\rangle|n\rangle, |V\rangle|n-1\rangle, |H\rangle|n-1\rangle, |B\rangle|n-2\rangle\}$, where $|n\rangle$ describes the state of the driving field with n photons. Since the laser is polarized in the vertical direction, the state $|H\rangle$ is not dressed by it, while the rest of the excitonic states are. The new eigenstates are obtained by diagonalizing the coupling Hamiltonian H_Ω (in the rotating frame of the laser) in the reduced basis $\{|G\rangle|n\rangle, |V\rangle|n-1\rangle, |B\rangle|n-2\rangle\}$, that is, the matrix:

$$H_{\text{TPE}} = \begin{pmatrix} 0 & \Omega & 0 \\ \Omega & \chi/2 & \Omega \\ 0 & \Omega & 0 \end{pmatrix}. \quad (9)$$

We do not include dissipation in this procedure since we consider it small as compared to Ω . This gives rise to the three new eigenvectors $\{|+\rangle, |0\rangle, |-\rangle\}$ in each rung with the corresponding eigenenergies:

$$\Delta_+ = \frac{1}{4}(\sqrt{\chi^2 + 32\Omega^2} + \chi), \quad (10a)$$

$$\Delta_0 = 0, \quad (10b)$$

$$\Delta_- = -\frac{1}{4}(\sqrt{\chi^2 + 32\Omega^2} - \chi), \quad (10c)$$

where the eigenvectors, dropping the photonic component from the notation, are given by $|+\rangle \propto |G\rangle + \Delta_+/\Omega|V\rangle + |B\rangle$, $|0\rangle = (|B\rangle - |V\rangle)/\sqrt{2}$ and $|-\rangle \propto |G\rangle + \Delta_-/\Omega|V\rangle + |B\rangle$. figure 1(b) depicts two successive rungs of excitation, including the state $|H\rangle$ which, as we said, remains bare.

3. Single photon transitions and spectrum

The spectrum of emission of the system in each polarization in the steady state, $S_X(\omega)$, with $X = H, V$, is defined as $S_X(\omega) = \Re \int_0^\infty \langle \sigma_X^\dagger(0) \sigma_X(\tau) \rangle e^{i\omega\tau} d\tau$. Both polarizations are plotted in figure 1(c) for comparison. The number of peaks appearing and their positions can be explained in each polarization X by the allowed single photon transitions under the operator σ_X . In the case of H polarization, only transitions between $|H\rangle$ and the dressed states $i = +, 0, -$ are allowed: $|\langle H| \sigma_H |i\rangle|^2 \neq 0$ or $|\langle i| \sigma_H |H\rangle|^2 \neq 0$. The transition $|H\rangle \rightarrow |H\rangle$ or between dressed states $|i\rangle \rightarrow |j\rangle$ is forbidden in H polarization, since $|\langle H| \sigma_H |H\rangle| = 0$ and $|\langle i| \sigma_H |j\rangle| = 0$ for all $i, j = +, 0, -$. The three possible transitions that can take place from the dressed states to $|H\rangle$, occur respectively at the following detunings from the laser (see figure 1(b)):

$$|+\rangle \rightarrow |H\rangle : \quad \Delta_I = \frac{1}{4}(\sqrt{\chi^2 + 32\Omega^2} - \chi), \quad (11a)$$

$$|0\rangle \rightarrow |H\rangle : \quad \Delta_{II} = -\chi/2, \quad (11b)$$

$$|-\rangle \rightarrow |H\rangle : \quad \Delta_{III} = -\frac{1}{4}(\sqrt{\chi^2 + 32\Omega^2} + \chi). \quad (11c)$$

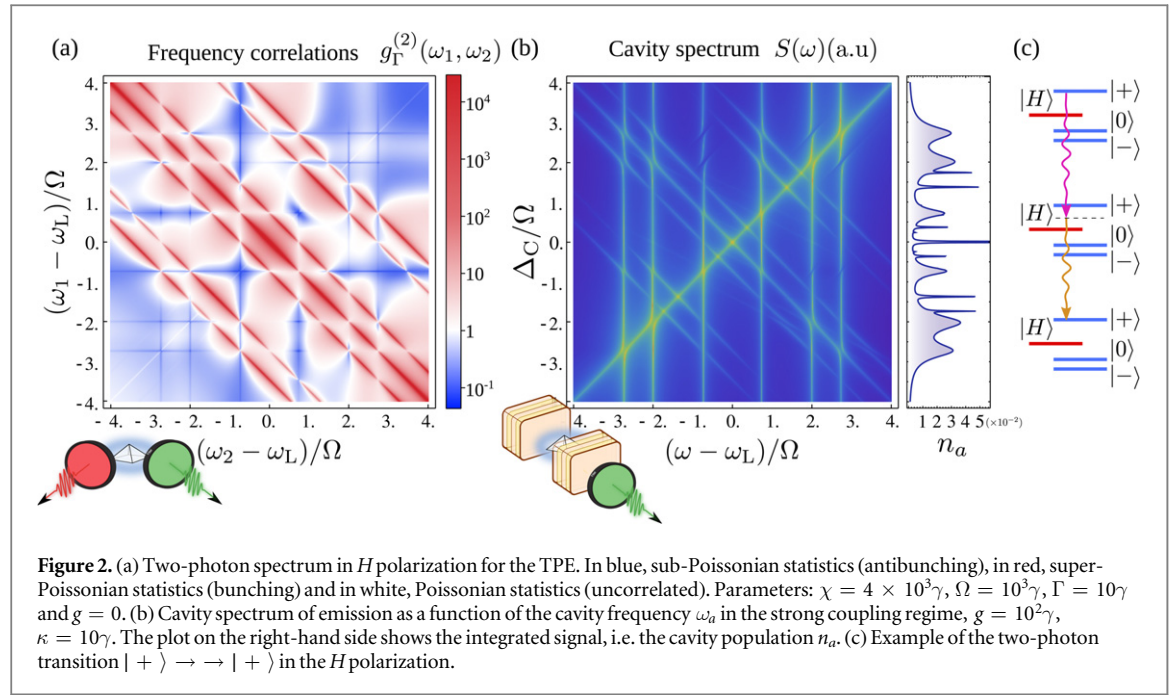
The other three possible H -polarized transitions take place from $|H\rangle$ to the dressed states, at opposite detunings $-\Delta_I, -\Delta_{II}$ and $-\Delta_{III}$. Remarkably, $S_H(\omega)$ does not present any resonance at the laser energy.

On the other hand, the spectrum in V polarization, $S_V(\omega)$, plotted with a dashed blue line in figure 1(c), contains seven peaks corresponding to the nine possible transitions between dressed states, $|i\rangle \rightarrow |j\rangle$, while those three between the same dressed states, $|i\rangle \rightarrow |i\rangle$, are degenerate in energy at ω_L .

4. Two-photon transitions and spectrum

The next step in the characterization of the system is the calculation of the frequency-resolved second order correlation function or two-photon spectrum, $g_\Gamma^{(2)}(\omega_1, \omega_2)$ [50, 51], which conveys how likely it is to detect two photons with frequencies ω_1, ω_2 simultaneously. For that purpose we use a recently developed technique [50] that makes the calculation of this quantity, previously very involved, computationally accessible, based on the inclusion of the detectors in the system dynamics. The parameter Γ is the inverse response time of the detector. It provides the frequency window in which photons are detected, around ω_1, ω_2 . We fix it to an intermediate value $\Gamma = 10\gamma$, so that the detectors can resolve full spectral peaks (with width of the order of γ) without resulting in superimposed signals, $\gamma < \Gamma \ll \Omega$.

Figure 2(a) shows the H -polarized two-photon spectrum from the light emitted by the dressed biexciton system. This map features seven antidiagonal red lines of super Poissonian correlations with $g_\Gamma^{(2)} \gg 1$ (hyperbunching) that correspond to a family of virtual two-photon processes that go from one state in a rung to



another state two rungs below, jumping over any states from the rung in between (whence the denomination of *leapfrog* processes). It was recently demonstrated [42] that this virtual character provides such strong quantum correlations that photon pairs can violate classical inequalities such as the Cauchy–Schwarz inequality.

Whenever any two of the frequencies involved correspond to transitions between real states, these correlations change character and the violation of Cauchy–Schwarz inequalities is spoiled. This can be seen in figure 2(a) as a piercing in the bunching lines whenever they intersect the vertical or horizontal ones, appearing at $\omega_{1,2} - \omega_L = \pm \Delta_I, \pm \Delta_{II}, \pm \Delta_{III}$.

Since the leapfrog lines originate from two-photon transitions, we can understand them in terms of the two-photon operator $\sigma_H \sigma_H$. Transitions starting or ending at $|H\rangle$ are not allowed, since $\langle H | \sigma_H \sigma_H | i \rangle = 0$ and $\langle i | \sigma_H \sigma_H | H \rangle = 0$. All other nine two-photon transitions, $|i\rangle \rightarrow \rightarrow |j\rangle$, occur, since $\langle j | \sigma_H \sigma_H | i \rangle \neq 0$ for all $i, j = +, 0, -$, and give rise to seven lines which follow the general equation $\omega_1 + \omega_2 - 2\omega_L = 2\Delta^{2P}$ with:

$$|i\rangle \rightarrow \rightarrow |i\rangle \quad \text{with} \quad i = +, 0, - : \quad \Delta_I^{2P} = 0, \quad (12a)$$

$$| + \rangle \rightarrow \rightarrow | 0 \rangle : \quad \Delta_{II}^{2P} = \frac{1}{8} \left(\sqrt{\chi^2 + 32\Omega^2} + \chi \right), \quad (12b)$$

$$| 0 \rangle \rightarrow \rightarrow | - \rangle : \quad \Delta_{III}^{2P} = \frac{1}{8} \left(\sqrt{\chi^2 + 32\Omega^2} - \chi \right), \quad (12c)$$

$$| + \rangle \rightarrow \rightarrow | - \rangle : \quad \Delta_{IV}^{2P} = \frac{1}{4} \sqrt{\chi^2 + 32\Omega^2}. \quad (12d)$$

The remaining three lines are described by inverting the order of the three last transitions and changing the sign of the corresponding Δ^{2P} . figure 2(c) shows an example of a two-photon transition, $| + \rangle \rightarrow \rightarrow | + \rangle$.

In figure 3, we have another view of these leapfrog resonances, selecting the diagonal of the two-photon spectrum in figure 2(a), that is, for $\omega = \omega_1 = \omega_2$. The leapfrog processes appear as seven lines around $\Omega/\chi \approx 10^{-1}$ and spread as Ω is increased. The blue lines correspond to the single-photon resonances that are also apparent in the spectrum of emission, cf figure 1(c). Reducing Ω below the dissipation levels (bottom part of the plot), the system experiences a transition into the spontaneous emission regime where there is no dressing of the levels and the spectral structures are much simpler: only two peaks for the spectrum of emission and a single leapfrog peak at $\omega = \omega_L$ in the two-photon spectrum. This regime was extensively investigated by one of the authors under incoherent excitation [40]. In the present work, where it appears as the low pumping limit, it will be used only for comparison with the high pumping regime.

5. Purcell enhancement of two-photon transitions by a cavity mode

These virtual leapfrog transitions can be made real by coupling the system to a cavity (we switch on $g \neq 0$) in resonance with at least one of the two frequencies involved. If the coupling is strong as compared to the cavity

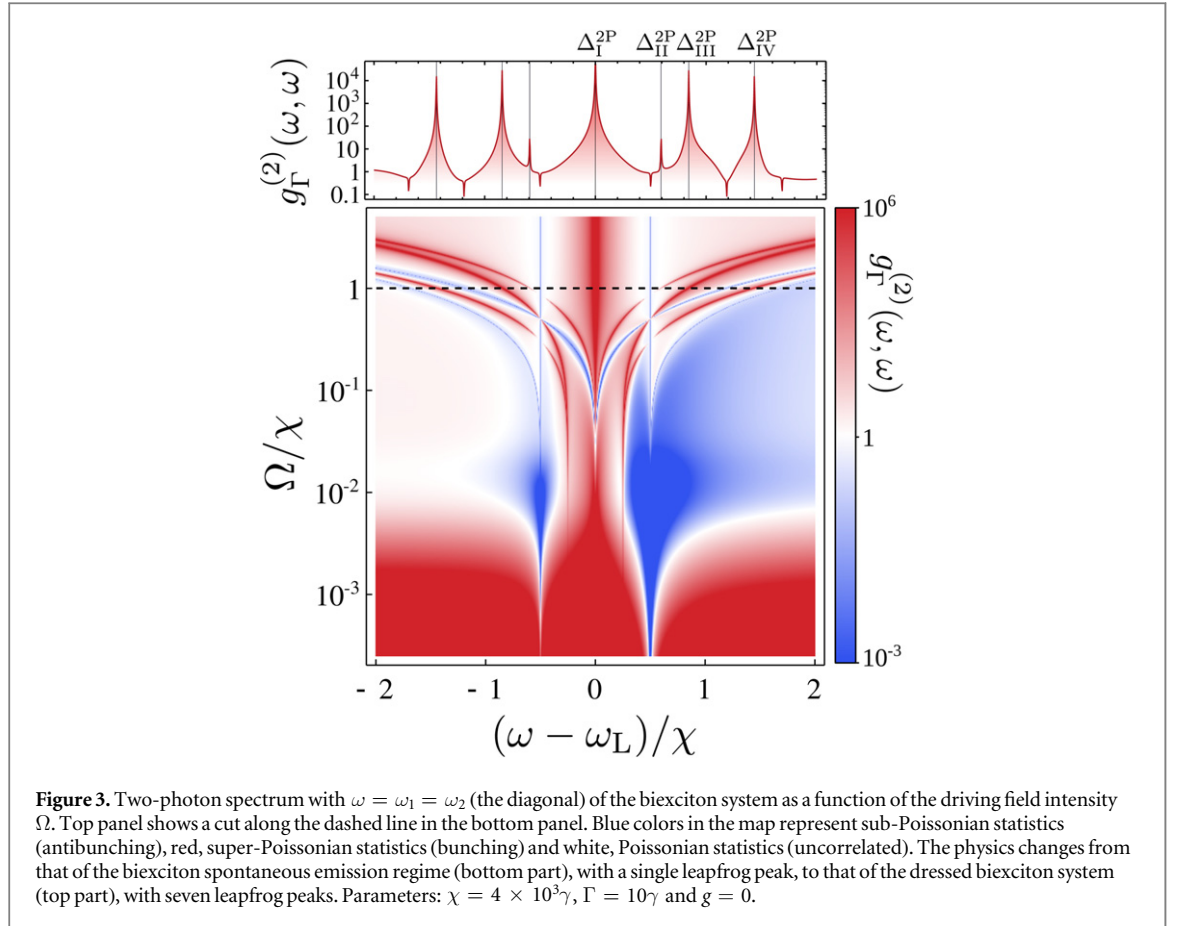


Figure 3. Two-photon spectrum with $\omega = \omega_1 = \omega_2$ (the diagonal) of the biexciton system as a function of the driving field intensity Ω . Top panel shows a cut along the dashed line in the bottom panel. Blue colors in the map represent sub-Poissonian statistics (antibunching), red, super-Poissonian statistics (bunching) and white, Poissonian statistics (uncorrelated). The physics changes from that of the biexciton spontaneous emission regime (bottom part), with a single leapfrog peak, to that of the dressed biexciton system (top part), with seven leapfrog peaks. Parameters: $\chi = 4 \times 10^3 \gamma$, $\Gamma = 10\gamma$ and $g = 0$.

dissipation, κ , the two-photon emission can be Purcell-enhanced. We can observe this in the cavity spectrum of emission, given by $S_a(\omega) = \Re \int_0^\infty \langle a^\dagger(0)a(\tau) \rangle e^{i\omega\tau} d\tau$ and plotted in figure 2(b). Because of the strong correlations between the two frequencies, the cavity Purcell enhancement of one of the two photons of a bunching line triggers the emission of the second photon, even if this one is not in resonance with the cavity. This phenomenon leaves traces in the spectrum that help reconstruct the bunching lines when the spectrum is plotted as a function of the cavity frequency. In this sense, the cavity is acting as one of the filters necessary to perform frequency correlations.

As we have shown with coworkers in a recent work [39], one can obtain useful two-photon emission by using this approach to Purcell enhance two photons of the same frequency. This is evidenced by sharp peaks in the cavity population whenever it crosses one of the two-photon resonances (equation (12) with $\omega_a = \omega_1 = \omega_2$), as can be seen in the right panel of figure 2(b). The single photon resonances appear as broad peaks and are detrimental for the two-photon emission. Therefore, the best candidates for pure two-photon emission are those leapfrogs far in energy from other processes, that is, the sharp peaks with small overlap with the (one-photon) broad one, which are further from the other (two-photon) sharp ones. Logically, it is also desirable that they are intense. The central peak, labelled I, at $\omega_a = \omega_L$ is the best candidate for that since it is the most isolated one and is degenerate, with contributions from three different leapfrog processes. As we will discuss, this has consequences on the statistics of the emitted pairs.

An accurate quantity to determine the quality of a two-photon resonance for two-photon emission is the *purity*, π_2 [39], defined as the fraction of photons emitted in pairs from the total emission (including single photons). Note that the purity being a probability, it is, unlike $g^{(2)}$, bounded: $0 \leq \pi_2 \leq 1$. Its definition is based on the fact that the photon counting distribution of a perfect two-photon emitter shows a suppressed probability of counting an odd number of photons. The details of its definition and computation can be found in the supplemental material. In order to compute it, we simulate the actual emission of the system in the steady state via a quantum Monte-Carlo method [39]. The result is plotted in figure 4(d) for a cavity on resonance with each of the leapfrog peaks in the two-photon spectrum: I, II, III and IV, whose positions shift with Ω as plotted in figure 4(e). The corresponding cavity population $n_a = \langle a^\dagger a \rangle$, second order correlation function $g^{(2)}(0) = \langle a^{\dagger 2} a^2 \rangle / n_a^2$ and two-photon second order correlation function [39] $g_2^{(2)}(0) = \langle a^{\dagger 4} a^4 \rangle / \langle a^{\dagger 2} a^2 \rangle^2$ appear

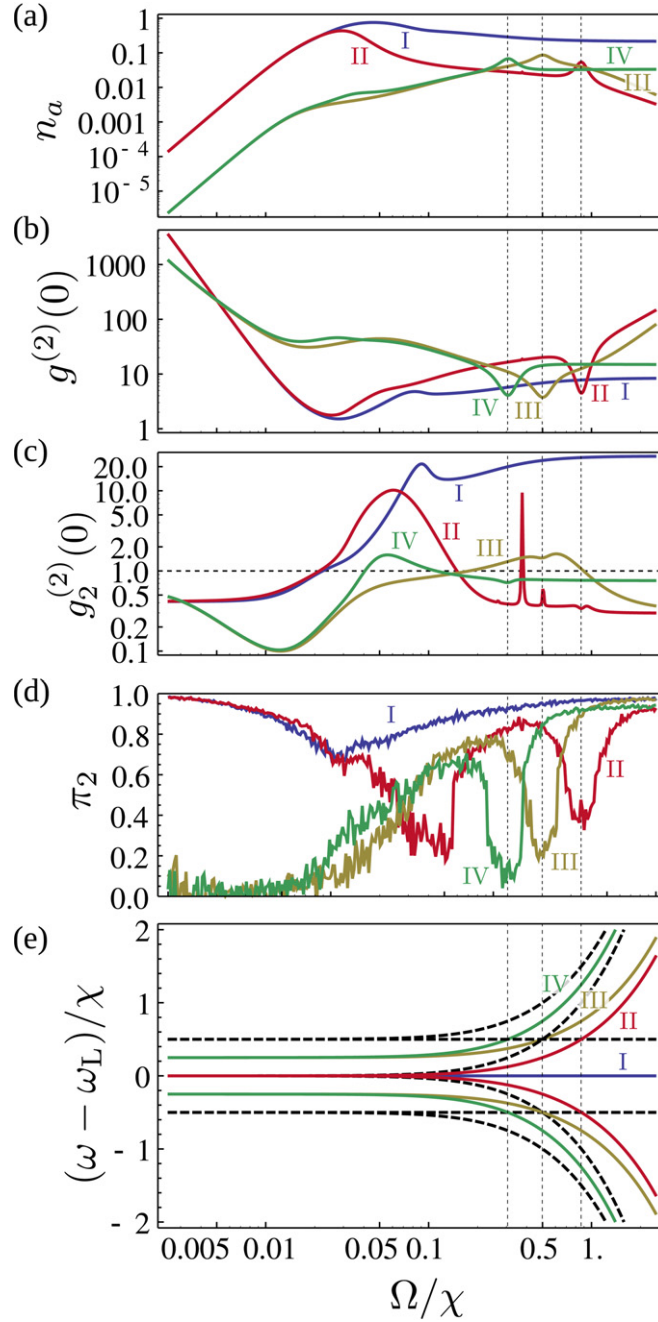


Figure 4. Steady state observables as a function of the pumping intensity Ω for the parameters: $\chi = 4 \times 10^3\gamma$, $g = 10^2\gamma$, $\kappa = 10\gamma$, $\Delta_X = \chi/2$ and $\Delta_C = \Delta_I^{2P}$ (blue), Δ_{II}^{2P} (red), Δ_{III}^{2P} (yellow) and Δ_{IV}^{2P} (green). The gridlines mark the three points where leapfrog processes intersect with real transitions—dashed lines in (e)—which spoils the purity.

in figures 4(a), (b) and (c) respectively. The latter quantity takes the meaning of a standard *second order correlation function for photon pairs* when these pairs dominate the emission ($\pi_2 \approx 1$).

In the low driving regime, we can see that resonances I and II converge to the same point at $\omega = \omega_L$ and show very high purity: this is the usual regime of two-photon emission in the (undressed) biexciton, that has been studied extensively before [52, 53]. Note, however, that this high purity comes at the expense of the amount of signal (low n_a). As figure 4 shows, this signal can be enhanced by orders of magnitude if we increase the pumping intensity Ω in order to bring the biexciton to the dressed regime. In this regime, all the resonances start being resolved and the four of them present a sizable purity. In the case of resonances II, III and IV, the purity goes down whenever they cross a single-photon resonance (dashed, vertical lines in figure 4). At very high intensity, $\Omega > \chi$, all of them reach almost 100% of pair emission.

In this limit of high pumping, we observe a bunching behaviour $g^{(2)}(0) > 1$ for all the leapfrog resonances, which is an expected result for two-photon emission. The statistics of the photons, however, hides a non-classical behaviour if one regards the pairs as the basic entity of emission and consider the pair–pair coincidences

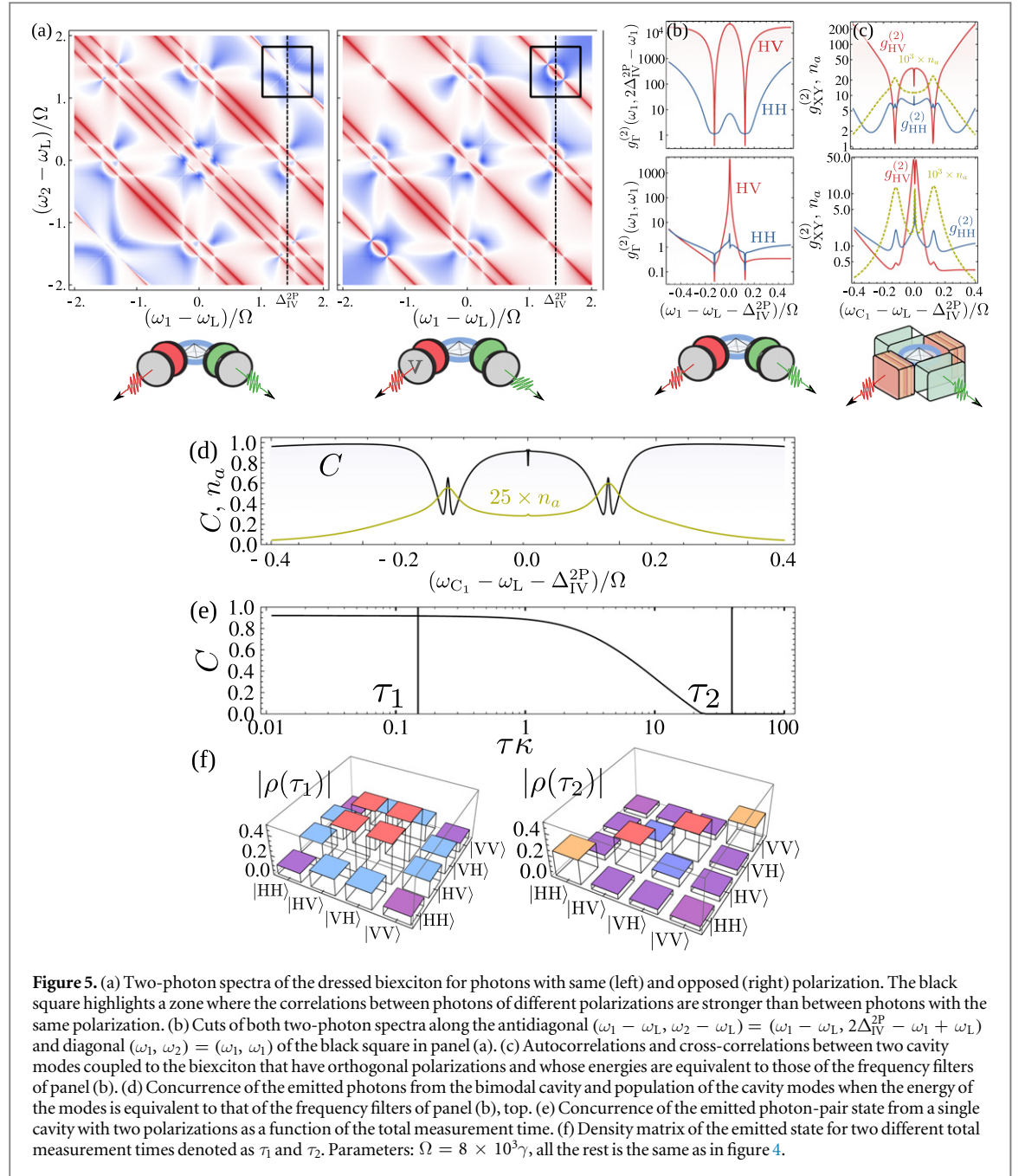
as described by the $g_2^{(2)}(0)$. In this case, we obtain *antibunched photon pairs* in resonances II, III and IV (giving the possibility of implementing an on-demand source of single photon pairs) and bunched photon pairs in resonance I. This is not the only difference between resonance I (blue) and the others. The position of this resonance is independent of the pumping intensity, and the emission at this frequency is orders of magnitude more intense than at the other resonances. These differences are explained by the fact that three different transitions contribute to the photon pair emission at line I, and that the starting and ending state of the transition are always the same, as can be seen in equation (12a). Because of this, no reloading time to go back to the initial state is needed, which is the origin of the antibunching on all the other cases. All these features are a sample of the rich set of physical regimes that can be explored when the proposed method of multi-photon Purcell enhancement in dressed states systems is applied in non-trivial configurations.

We will now compare the emission rates that can be obtained through this mechanism with other approaches in similar systems. The most straightforward comparison is with the undressed regime [35]. For the parameters used in figure 4(b), for the minimum (undressed regime) and maximum (dressed regime) values of Ω shown on the figure, we obtain $n_a = 2 \times 10^{-4}$ and $n_a = 0.25$, respectively, which for $g = 51 \mu\text{eV}$ [35] gives pair generation rates of $r = 0.12 \text{ MHz}$ and $r = 151 \text{ MHz}$, that is, over three orders of magnitude enhancement. While this comparison is illustrative of the gain brought by our paradigm, it does not represent an exhaustive study of the space of parameters. For instance, resonances II, III and IV benefit from higher values of γ than those studied here, leading to faster reloading times that increase the value of n_a . For a fixed g , changes in χ , κ or γ can optimize the generation rates of either regime, although the dressed case should typically outperform the undressed one. A comparison can also be made with proposals in the pulsed excitation regime, although the juxtaposition with our continuous-wave excitation case is less direct. We will compare with the rates obtained in [27, 28], since both works use the biexcitonic cascade to generate photon pairs. For this analysis, since we compare with existing experiments, we use parameters of systems available in the laboratory, namely $g = 51 \mu\text{eV}$, $\kappa = 24 \mu\text{eV}$ and $\gamma = 0.13 \mu\text{eV}$ [35], along with $\chi = 2 \text{ meV}$ [28]. Doing so is detrimental to our proposal that exploits the strong-coupling regime [39] and performs better with figures of merit not yet available in the laboratory, but which remain realistic in the light of the technological progress in growth and materials science. Still, in units normalized to g , this choice of today's parameters for our mechanism yield $\kappa \approx 0.5 g$, $\gamma \approx 0.002 g$ and $\chi \approx 40 g$. We will focus on resonance I, which is the brightest. For these parameters and high values of the pumping, $\Omega \approx 2.5\chi$, the cavity acquires a population $n_a \approx 0.01$ and a top purity of pair emission, $\pi_2 \approx 1$, with a photon pair generation rate of $r = n_a \kappa / 2 \approx 29 \text{ MHz}$. This is superior to both the values obtained in [27], with $r = 10 \text{ MHz}$, where a Purcell enhancement through cavity modes is also used, and in [28], with $r = 0.3 \text{ MHz}$. The last work actually reports a higher generation rate but correcting for their collection efficiency of $\approx 0.4\%$, since light is emitted isotropically from a quantum dot. In contrast, our proposal, like the one in [27], collects the light through the cavity channel, therefore solving this problem. Notice as well that said collection through the cavity mode is done by Purcell enhancing a two-photon process of photons with equal energy, that in consequence will be indistinguishable. This represents another advantage with respect to the conventional approach based on emission from the bare biexcitonic states, which might suffer from fine-structure splitting, spoiling indistinguishability.

6. Emission of entangled photons

Many practical applications in quantum computing and quantum communication require emission of entangled photon pairs [3, 5–11]. So far, we have only considered the case in which the emission was filtered by a single cavity with a fixed polarization. Therefore, changing the frequency of the cavity corresponds to moving along the diagonal of figure 2(a), and all photons extracted by the cavity will tend to be indistinguishable. However, the results for the spectrum of the cavity emission depicted in figure 2(b) show that correlated photons of different frequencies can be Purcell enhanced with a single cavity, so that the spectrum as a function of the cavity detuning follows the trend of the two-photon frequency correlation map of the biexciton, figure 2(a). It is therefore expected that a bimodal cavity in resonance with two different, correlated frequencies—showing bunching in the map of figure 2(a)—will show strongly correlated emission. The biexcitonic scheme also allows us to introduce an extra degree of freedom, the polarization, such that two-photon emission takes place in a reduced Hilbert space of polarization and frequency $\{|H, \omega_1; H, \omega_2\rangle, |H, \omega_1; V, \omega_2\rangle, |V, \omega_1; H, \omega_2\rangle, |V, \omega_1; V, \omega_2\rangle\}$. We will now show how the mechanism of two-photon emission described above can be extended to yield emission of entangled photons of the kind $|\psi\rangle = (|H, \omega_1; V, \omega_2\rangle + |V, \omega_1; H, \omega_2\rangle) / \sqrt{2}$ when the enhancement of the light emitted by the dressed biexciton is done by a bimodal cavity, with each of the modes having two degenerate polarizations.

The system, already implemented experimentally [27, 54] is theoretically described in the same way as before, but now including including four cavity modes with annihilation operator $a_{i,X}$, $i \in \{1, 2\}$,



$X \in \{H, V\}$, describing the two possible polarizations of the two modes of the bimodal cavity. The part of the Hamiltonian that describes the cavity modes and their coupling to the biexciton is then given by:

$$\begin{aligned}
 H_C = & \omega_{C_1}(a_{1,H}^\dagger a_{1,H} + a_{1,V}^\dagger a_{1,V}) \\
 & + \omega_{C_2}(a_{2,H}^\dagger a_{2,H} + a_{2,V}^\dagger a_{2,V}) \\
 & + g[(a_{1,H}^\dagger + a_{2,H}^\dagger)\sigma_H + (a_{1,H} + a_{2,H})\sigma_H^\dagger] \\
 & + g[(a_{1,V}^\dagger + a_{2,V}^\dagger)\sigma_V + (a_{1,V} + a_{2,V})\sigma_V^\dagger].
 \end{aligned} \tag{13}$$

The vertically polarized driving term given by equation (4) leads to different probability of emission in horizontal or vertical polarization. Since we now want that probability to be equal, we use a circularly polarized driving laser:

$$H_\Omega = \Omega(\sigma_\circ^\dagger e^{-i\omega_L t} + \sigma_\circ e^{i\omega_L t}) \tag{14}$$

with $\sigma_\circ = (\sigma_H + i\sigma_V)/\sqrt{2}$. We will not discuss in detail the possible single and two-photon transitions that arise in the dressed biexciton under this driving, since the physics and derivation are similar to the results presented above for the linearly polarized pumping. However, it is interesting to analyze the frequency-resolved,

cross-polarized second order correlation function $g_{\Gamma, HV}^{(2)}(\omega_1, \omega_2)$ of the dressed biexcitonic system alone ($g = 0$), which is a cross-correlation function between photons emitted at frequency ω_1 and polarization H and photons emitted at frequencies ω_2 and polarization V . This correlation function can be compared with the frequency-resolved correlation functions for a fixed polarization that we have been considering so far, that we now term $g_{\Gamma, HH}^{(2)}(\omega_1, \omega_2)$. Due to the circular polarized pumping, the system is symmetric under the exchange $H \leftrightarrow V$, so $g_{\Gamma, HH}^{(2)}(\omega_1, \omega_2) = g_{\Gamma, VV}^{(2)}(\omega_1, \omega_2)$ and $g_{\Gamma, HV}^{(2)}(\omega_1, \omega_2) = g_{\Gamma, VH}^{(2)}(\omega_1, \omega_2)$.

Figure 5(a) shows the comparison between these two quantities. While $g_{\Gamma, HH}^{(2)}$ displays the same features as in the case of linearly polarized pumping (figure 2(a)), the cross-polarized correlation function $g_{\Gamma, HV}^{(2)}$ presents a leapfrog line Δ_{IV}^{2P} where correlations are much stronger than in the case of photons emitted with the same polarization. The region where this happens is highlighted with a black square on the map. Figure 5(b) shows a cut of both $g_{\Gamma, HH}^{(2)}$ and $g_{\Gamma, HV}^{(2)}$ on the diagonal (ω, ω) of the black square and the antidiagonal $(\omega, 2\Delta_{IV}^{2P} - \omega)$, corresponding to said leapfrog line of strong correlations. These curves show that, when the light is filtered at two frequencies along this line, emission of photons of different polarization is clearly dominant over the emission of photons of equal polarization. The dip in the correlations corresponds to the crossing with a single-photon transition. This behaviour is mapped onto the emission of the bimodal cavity when the frequencies of the modes correspond to those of the filters, as is shown in figure 5(c), which depicts the correlations between the two modes (for the same and different polarizations) when their frequencies are the same as those of the frequency filters of panel (b). The population of the modes is also shown, featuring in the bottom panel a sharp resonance when the two modes have equal frequency and the two-photon resonance is crossed. The top panel shows how, as the separation in frequency between the modes increases (always maintained in the line of strong correlations), the population decreases after crossing the single photon resonance. However, a strong difference on the correlations between similar and different polarizations can be achieved without paying too much attention to the signal, yielding much better entanglement, as we show below.

Quantum tomography [27, 40, 55, 56] allows us to reconstruct the density matrix of the emitted photon pairs in the basis $\{|H, \omega_1; H, \omega_2\rangle, |H, \omega_1; V, \omega_2\rangle, |V, \omega_1; H, \omega_2\rangle, |V, \omega_1; V, \omega_2\rangle\}$ from second order correlation functions corresponding to photon coincidence measurements. We define the (unnormalized) density matrix:

$$\theta_{AB, CD} = \langle a_A^\dagger a_B^\dagger a_D a_C \rangle \quad (15)$$

with $\{A, C\} \equiv \{A, \omega_1; C, \omega_1\}$, $\{B, D\} \equiv \{B, \omega_2; D, \omega_2\}$ and $A, B, C, D \in \{H, V\}$. The corresponding normalized density matrix is $\tilde{\theta} = \theta / \text{Tr}[\theta]$. The degree of entanglement of this emitted bipartite state can be quantified by the concurrence C ³, that in the case of pure states ranges from 0 (separable states) to 1 (maximally entangled states) [58]. Figure 5(d) depicts the concurrence of the emitted states as the frequencies of the modes move along the leapfrog line of strong correlations, $(\omega_{C_1} - \omega_L, \omega_{C_2} - \omega_L) = (\omega_{C_1} - \omega_L, 2\Delta_{IV}^{2P} - \omega_{C_1} + \omega_L)$, corresponding to the same points shown in figure 5(c), top. A region of concurrence $C \approx 0.9$ exists for small detuning between the two modes, while another region where $C \approx 1$ can be reached for higher energy differences without a dramatic decrease in the rate of emission, as can be seen in the behaviour of n_a (which is the population of one of the modes, all of them being equally populated). These high values of the concurrence correspond to the emission of photons in a pure entangled Bell state $|\psi\rangle = (|H, \omega_1; V, \omega_2\rangle + |V, \omega_1; H, \omega_2\rangle) / \sqrt{2}$.

Entanglement can also be studied for a single cavity mode with two polarizations, with time of emission being the extra degree of freedom instead of frequency. In that case, the states of the Hilbert space are of the form $|X Y\rangle \equiv |X, \text{early}; Y, \text{late}\rangle$, with $X, Y \in \{H, V\}$. The density matrix is then defined as [40, 56]

$$\theta_{AB, CD}(\tau) = \int_0^\tau \langle a_A^\dagger(0) a_B^\dagger(\tau') a_D(\tau') a_C(0) \rangle d\tau' \quad (16)$$

with $A, B, C, D \in \{H, V\}$, and two-time correlation functions are calculated from the steady state of the system using the quantum regression theorem [57]. Therefore, τ corresponds to the time of measurement that begins with the emission of the first photon, and for each τ we define the normalized density matrix $\tilde{\theta}(\tau) = \theta(\tau) / \text{Tr}[\theta(\tau)]$. This analysis reveals, for short measurement times, a highly pure density matrix, $\text{Tr}[\tilde{\theta}^2] \approx 0.92$ consisting of the entangled Bell state $|\psi\rangle = (|HV\rangle + |VH\rangle) / \sqrt{2}$ with fidelity $F \approx 0.9$, shown in figure 5(e). Beyond a certain time of measurement $1/\kappa$, the density matrix loses purity due to the contributions from subsequent emissions. In our configuration, the concurrence takes a value $C \approx 0.92$ for short measurement times. However, one must bear in mind that the maximum concurrence for a mixed state is lower than one [59] and $\tilde{\theta}$ is a mixed state with linear entropy $S_L(\theta) = 4/3[1 - \text{Tr}(\theta^2)] \approx 0.11$, which brings this value of C closer to that of a maximally entangled mixed state. These results, which come from a specific choice of parameters and therefore do not represent an exhaustive study of all the scenarios available, prove

³ This quantity is defined as $C = \max\{0, \sqrt{\lambda_1} - \sqrt{\lambda_2} - \sqrt{\lambda_3} - \sqrt{\lambda_4}\}$, where $\{\lambda_1, \lambda_2, \lambda_3, \lambda_4\}$ are the eigenvalues in decreasing order of the matrix $\rho T \rho^* T$, with T a diagonal matrix with diagonal $\{-1, 1, 1, -1\}$.

unambiguously that the mechanism of two-photon emission analyzed in this text can be easily extended to include new degrees of freedom—like color or polarization—and provide entangled two-photon emission.

7. Conclusions

We have shown how Purcell enhancement of multi-photon resonances in the dressed ladder of a strongly driven biexciton can yield regimes of bright continuous two-photon emission. Thanks to the strong driving, the emission of photon pairs occurs at a much higher rate than it would in the approach that combines standard two-photon excitation (without dressing the system) and two-photon Purcell enhancement. The richness of the dressed biexcitonic structure allows us to reach different two-photon regimes like antibunched two-photon emission or polarization and frequency (or time) entangled photon pairs. These results suggest that the fundamental ideas behind this particular proposal are susceptible to be applied in a variety of platforms.

Acknowledgements

We acknowledge the IEF project SQUIRREL (623708), the Spanish MINECO (MAT2011–22997, MAT2014–53119-C2–1-R, FPI & RyC programs) and the ERC POLAFLOW.

References

- [1] O'Brien J L, Furusawa A and Vuckovic J 2009 Photonic quantum technologies *Nat. Phys.* **3** 687
- [2] Knill E, Laflamme R and Milburn G J 2001 A scheme for efficient quantum computation with linear optics *Nature* **409** 46–52
- [3] Pan J-W et al 2012 Multiphoton entanglement and interferometry *Rev. Mod. Phys.* **84** 777
- [4] Hong C K and Mandel L 1986 Experimental realization of a localized one-photon state *Phys. Rev. Lett.* **56** 58
- [5] Jennewein T, Simon C, Weihs G, Weinfurter H and Zeilinger A 2000 Quantum cryptography with entangled photons *Phys. Rev. Lett.* **84** 4729
- [6] Naik D S, Peterson C G, White A G, Berglund A J and Kwiat P G 2000 Entangled state quantum cryptography: Eavesdropping on the Ekert protocol *Phys. Rev. Lett.* **84** 4733
- [7] Bouwmeester D et al 1997 Experimental quantum teleportation *Nature* **390** 575
- [8] Marcikic I, Riedmatten H D, Tittel W, Zbinden H and Gisin N 2003 Long-distance teleportation of qubits at telecommunication wavelengths *Nature* **421** 509
- [9] Pan J-W, Bouwmeester D, Weinfurter H and Zeilinger A 1998 Experimental entanglement swapping: Entangling photons that never interacted *Phys. Rev. Lett.* **80** 3891
- [10] Simon C et al 2007 Quantum repeaters with photon pair sources and multimode memories *Phys. Rev. Lett.* **98** 190503
- [11] Troiani F 2014 Entanglement swapping with energy-polarization-entangled photons from quantum dot cascade decay *Phys. Rev. B* **90** 245419
- [12] Giovannetti V, Lloyd S and Maccone L 2004 Quantum-enhanced measurements: Beating the standard quantum limit *Science* **306** 1330
- [13] Gea-Banacloche J 1989 Two-photon absorption of nonclassical light *Phys. Rev. Lett.* **62** 1603
- [14] Upton L et al 2013 Optically excited entangled states in organic molecules illuminate the dark *The Journal of Physical Chemistry Letters* **4** 2046–52
- [15] Peruzzo A et al 2010 Quantum walks of correlated photons *Science* **329** 1500
- [16] Lanyon B P et al 2010 Towards quantum chemistry on a quantum computer *Nat. Chem* **2** 106
- [17] Burnham D C and Weinberg D L 1970 Observation of simultaneity in parametric production of optical photon pairs *Phys. Rev. Lett.* **25** 84
- [18] Kwiat P G et al 1995 New high-intensity source of polarization-entangled photon pairs *Phys. Rev. Lett.* **75** 4337
- [19] Lanco L et al 2006 Semiconductor waveguide source of counterpropagating twin photons *Phys. Rev. Lett.* **97** 173901
- [20] Horn R et al 2012 Monolithic source of photon pairs *Phys. Rev. Lett.* **108** 153605
- [21] Boitier F et al 2014 Electrically injected photon-pair source at room temperature *Phys. Rev. Lett.* **112** 183901
- [22] Scarani V, Riedmatten H D, Marcikic I, Zbinden H and Gisin N 2005 Four-photon correction in two-photon bell experiments *Eur. Phys. J. D* **32** 129
- [23] Aspect A, Grangier P and Roger G 1981 Experimental tests of realistic local theories via Bell's theorem *Phys. Rev. Lett.* **47** 460
- [24] Stevenson R M et al 2006 A semiconductor source of triggered entangled photon pairs *Nature* **439** 179
- [25] Akopian N et al 2006 Entangled photon pairs from semiconductor quantum dots *Phys. Rev. Lett.* **96** 130501
- [26] Hafenbrak R et al 2007 Triggered polarization-entangled photon pairs from a single quantum dot up to 30K *New J. Phys.* **9** 315
- [27] Dousse A et al 2010 Ultrabright source of entangled photon pairs *Nature* **466** 217
- [28] Müller M, Bounouar S, Jöns K D, Gläsel M and Michler P 2014 On-demand generation of indistinguishable polarization-entangled photon pairs *Nat. Photon* **8** 224–8
- [29] Flissikowski T, Betke A, Akimov I A and Henneberger F 2004 Two-photon coherent control of a single quantum dot *Phys. Rev. Lett.* **92** 227401
- [30] Stuffer S et al 2006 Two-photon Rabi oscillations in a single $\text{In}_x\text{Ga}_{1-x}\text{As}/\text{GaAs}$ quantum dot *Phys. Rev. B* **73** 125304
- [31] Jayakumar H et al 2013 Deterministic photon pairs and coherent optical control of a single quantum dot *Phys. Rev. Lett.* **110** 135505
- [32] Huber T et al 2015 Coherence and degree of time-bin entanglement from quantum dots arXiv:1506.02429
- [33] Birowosuto M D et al 2012 Fast purcell-enhanced single photon source in 1.550-nm telecom band from a resonant quantum dot-cavity coupling *Sci. Rep.* **2**
- [34] del Valle E et al 2010 Two-photon lasing by a single quantum dot in a high-Q microcavity *Phys. Rev. B* **81** 035302
- [35] Ota Y, Iwamoto S, Kumagai N and Arakawa Y 2011 Spontaneous two-photon emission from a single quantum dot *Phys. Rev. Lett.* **107** 233602

- [36] Schumacher S *et al* 2012 Cavity-assisted emission of polarization-entangled photons from biexcitons in quantum dots with fine-structure splitting *Opt. Express* **20** 5335
- [37] Cohen-Tannoudji C N and Reynaud S 1977 Dressed-atom description of resonance fluorescence and absorption spectra of a multi-level atom in an intense laser beam *J. Phys. B.: At. Mol. Phys.* **10** 345
- [38] Muller A, Fang W, Lawall J and Solomon G S 2008 Emission spectrum of a dressed exciton-biexciton complex in a semiconductor quantum dot *Phys. Rev. Lett.* **101** 027401
- [39] Sánchez Muñoz C *et al* 2014 Emitters of N-photon bundles *Nat. Photon* **8** 550
- [40] del Valle E 2013 Distilling one, two and entangled pairs of photons from a quantum dot with cavity QED effects and spectral filtering *New J. Phys.* **15** 025019
- [41] Gonzalez-Tudela A, del Valle E and Laussy F P 2015 Optimization of photon correlations by frequency filtering *Phys. Rev. A* **91** 043807
- [42] Sánchez Muñoz C, del Valle E, Tejedor C and Laussy F P 2014 Violation of classical inequalities by photon frequency filtering *Phys. Rev. A* **90** 052111
- [43] Peiris M *et al* 2015 Two-color photon correlations of the light scattered by a quantum dot *Phys. Rev. B* **91** 195125
- [44] Quang T and Freedhoff H 1993 Atomic population inversion and enhancement of resonance fluorescence in a cavity *Phys. Rev. A* **47** 2285
- [45] Kim H, Shen T C, Roy-Choudhury K, Solomon G S and Waks E 2014 Resonant interactions between a mollow triplet sideband and a strongly coupled cavity *Phys. Rev. Lett.* **113** 027403
- [46] Aspect A, Roger G, Reynaud S, Dalibard J and Cohen-Tannoudji C 1980 Time correlations between the two sidebands of the resonance fluorescence triplet *Phys. Rev. Lett.* **45** 617
- [47] Schrama C A, Nienhuis G, Dijkerman H A, Steijsiger C and Heideman H G M 1992 Intensity correlations between the components of the resonance fluorescence triplet *Phys. Rev. A* **45** 8045
- [48] Ulhaq A *et al* 2012 Cascaded single-photon emission from the Mollow triplet sidebands of a quantum dot *Nat. Photon* **6** 238
- [49] Baur M *et al* 2009 Measurement of Autler-Townes and Mollow transitions in a strongly driven superconducting qubit *Phys. Rev. Lett.* **102** 243602
- [50] del Valle E, Gonzalez-Tudela A, Laussy F P, Tejedor C and Hartmann M J 2012 Theory of frequency-filtered and time-resolved n-photon correlations *Phys. Rev. Lett.* **109** 183601
- [51] Gonzalez-Tudela A, Laussy F P, Tejedor C, Hartmann M J and del Valle E 2013 Two-photon spectra of quantum emitters *New J. Phys.* **15** 033036
- [52] del Valle E, Gonzalez-Tudela A, Cancellieri E, Laussy F P and Tejedor C 2011 Generation of a two-photon state from a quantum dot in a microcavity *New J. Phys.* **13** 113014
- [53] del Valle E, Gonzalez-Tudela A and Laussy F P 2012 Generation of a two-photon state from a quantum dot in a microcavity under incoherent and coherent continuous excitation *Proc. SPIE Physics and Simulation of Optoelectronic Devices XX* **8255** 825505
- [54] Kress A *et al* 2005 Manipulation of the spontaneous emission dynamics of quantum dots in two-dimensional photonic crystals *Phys. Rev. B* **71** 241304
- [55] James D F V, Kwiat P G, Munro W J and White A G 2001 Measurement of qubits *Phys. Rev. A* **64** 52312
- [56] Troiani F, Perea J I and Tejedor C 2006 Cavity-assisted generation of entangled photon pairs by quantum dot cascade decay *Phys. Rev. B* **74** 235310
- [57] Scully M O and Zubairy M S 2002 *Quantum optics* (Cambridge: Cambridge University Press)
- [58] Wootters W K 1998 Entanglement of formation of an arbitrary state of two qubits *Phys. Rev. Lett.* **80** 2245
- [59] Wei T C *et al* 2003 Maximal entanglement versus entropy for mixed quantum states *Phys. Rev. A* **67** 022110